



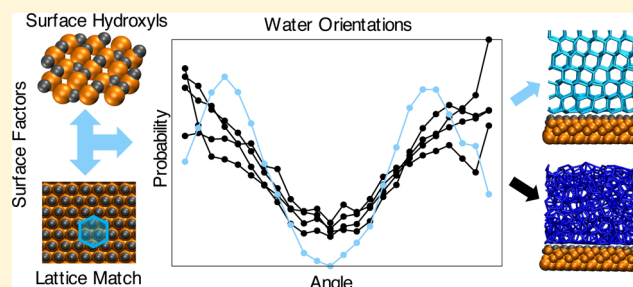
Heterogeneous Ice Nucleation: Interplay of Surface Properties and Their Impact on Water Orientations

Brittany Glatz and Sapna Sarupria*

Department of Chemical & Biomolecular Engineering, Clemson University, Clemson, South Carolina 29634, United States

 Supporting Information

ABSTRACT: Ice is ubiquitous in nature, and heterogeneous ice nucleation is the most common pathway of ice formation. How surface properties affect the propensity to observe ice nucleation on that surface remains an open question. We present results of molecular dynamics studies of heterogeneous ice nucleation on model surfaces. The model surfaces considered emulate the chemistry of kaolinite, an abundant component of mineral dust. We investigate the interplay of surface lattice and hydrogen bonding properties in affecting ice nucleation. We find that lattice matching and hydrogen bonding are necessary but not sufficient conditions for observing ice nucleation at these surfaces. We correlate this behavior to the orientations sampled by the metastable supercooled water in contact with the surfaces. We find that ice is observed in cases where water molecules not only sample orientations favorable for bilayer formation but also do not sample unfavorable orientations. This distribution depends on both surface–water and water–water interactions and can change with subtle modifications to the surface properties. Our results provide insights into the diverse behavior of ice nucleation observed at different surfaces and highlight the complexity in elucidating heterogeneous ice nucleation.



1. INTRODUCTION

Heterogeneous ice nucleation is one of the dominant pathways for ice formation relevant to a variety of fields, such as microbiology,^{1–4} water transport in plants,⁵ food preservation,⁶ and atmospheric studies.^{7,8} Heterogeneous ice nucleation can occur at warmer temperatures than required for homogeneous ice nucleation, making it the more commonly observed phenomena.^{7,9,10} Different surfaces promote ice nucleation at different temperatures and rates.^{4,9,11–17} Although these differences are documented, there is no explanation for the disparity of surface effects on ice nucleation. Additionally, the mechanisms underlying a surface's ability to promote ice nucleation are unknown. Therefore, it is imperative to probe the relation between the surface and water behavior at supercooled temperatures to bring us closer to answering these open questions. Studying ice formation on common nucleants is an important step in establishing such relations.

Several field studies and experimental efforts have characterized the ice nucleating efficiency of various surfaces relevant to atmospheric ice nucleation.^{7,9,10,14,18,19} The studies indicate that mineral dust particles such as kaolinite, Illite, quartz and montmorillonite catalyze ice nucleation.^{9,14,19,20} While experiments provide insights into the ice nucleating ability of different surfaces, they struggle to provide molecular details. On the other hand, molecular simulations can provide these details for water–surface interactions. Recently, several simulation studies have been reported on water adsorption and ice nucleation near various surfaces.^{15,16,21–41} Simulations show that templating alone does not account for a surface's ice nucleating

ability.^{15,16,23,30,31,33–35,37,39–44} Based on ice nucleation simulations on generic (graphite-like) surfaces, different theories in addition to templating have been put forth to explain the ice nucleating abilities of surfaces.^{23,30,31,44} One theory suggests that there is an optimum strength of interaction between the surface and the water molecules that stabilizes ice-like configurations near the surface thereby promoting ice nucleation.^{30,31} Another explanation contends that an increased layering of water molecules caused by the surface promotes ice nucleation.^{23,44} However, it has been found that neither of these theories readily transfer to other surfaces, highlighting the complexity of heterogeneous ice nucleation.^{31,33,35,37} As ice nucleation mechanisms vary in accordance with the surface, more nucleants need to be studied.

One surface that has been the focus of several recent simulation studies is kaolinite.^{22,35,42,45} Kaolinite is one of the most abundant mineral dust particles in the atmosphere, accounting for as much as 75% of mineral dust in some areas.^{7,46} Kaolinite is a layered aluminosilicate mineral and exposes a layer of hydroxyl groups arranged in a hexagonal pattern on the (001) plane. According to the conventional explanation, ice nucleation is promoted since this hexagonal arrangement templates the basal plane of ice. However, this has

Special Issue: Early Career Authors in Fundamental Colloid and Interface Science

Received: August 12, 2017

Revised: October 9, 2017

Published: October 11, 2017

been contested in recent simulations. Using first-principles calculations, Hu and Michaelides²⁹ concluded that the ice nucleating efficiency of kaolinite is attributable to its ability to hydrogen bond with water molecules. It has been suggested that the ability of the hydroxyl groups on the surface to respond to the water structure is a factor in kaolinite's ice nucleating ability.⁴² Furthermore, the hydroxyl-terminated surface of kaolinite was found to nucleate ice on the prismatic plane in contrast to the expected basal plane.^{22,42,43} Additionally, slight changes to the surface or including the vibrations of surface atoms seem to hinder ice nucleation altogether in kaolinite.⁴⁵ Collectively, this demonstrates an delicate interplay of different surface properties in promoting ice nucleation.

To elucidate the interplay of surface properties on ice nucleation, we investigate the role of lattice matching and hydrogen bonding on model surfaces. The model surfaces emulate the chemical structure of kaolinite. We perform extensive microsecond long molecular dynamics (MD) simulations of the water-surface systems. Our results establish that in kaolinite-like surfaces lattice matching and hydrogen bonding are necessary but not sufficient conditions to promote ice nucleation. Furthermore, consistent with our previous study³⁷ we observe a correlation between the orientation distribution of interfacial water molecules in the metastable liquid and the propensity of observing ice nucleation.

2. SIMULATION METHODS

We investigate the effects of surface lattice spacing and hydrogen bonding ability on ice nucleation through microsecond-long MD simulations of water near model mineral surfaces. The model surfaces are generated based on the chemical structure of kaolinite. Kaolinite is comprised of a tetrahedral SiO_4 layer bonded to an octahedral aluminum (AlO_6) layer. The oxygen atoms that are bonded to aluminum atoms and not shared with the silicon atoms are hydroxylated, resulting in a layer of hydroxyl groups on the (001) plane.

Our model surfaces are generated to emulate the kaolinite chemical structure. However, they are designed such that the resulting hydroxyl layer is planar with the oxygen atoms arranged in a regular hexagonal packing. This was achieved by using an average Al–O bond distance of 1.907 Å^{47,48} in generating the structure with similar geometry to kaolinite. We refer to these model surfaces as kao surfaces henceforth. Previous studies have suggested that the corrugation of the kaolinite surface could play a role in ice nucleation.⁴⁵ Using kao as our model surfaces enables us to eliminate this effect and focus specifically on the interplay of lattice matching and hydrogen bonding. Further details of the kao structure are provided in the [Supporting Information](#).

Modified kao surfaces were generated by expanding or compressing our model kao structure by 10 and 20%. We refer to these surfaces as $\text{kao}_{x,n}$ where x is “+” for stretched (increased distances) and “−” for compressed (decreased distances) surfaces, and n represents the percent change in the atom distances. This resulted in a total of five different surfaces ([Table 2](#)). The kao_{-20} surface has a lattice spacing that presents a perfect match to the basal plane of the ice structure.

Each simulation system comprised of two slabs of kao, where each slab is composed of two kao layers. The slabs are placed such that they mirror each other to prevent the artifacts resulting from the unphysical, long-range electric fields caused by lattice truncation.^{25,49} Water molecules were placed in contact with the exposed hydroxyl layer of each slab. The distance between the two water layers in the starting configuration was maintained to be at least 2 nm to minimize the interactions between them and allow for the density fluctuations inherent to ice nucleation. The box dimensions varied from $2.7 \times 2.3 \times 22.6 \text{ nm}^3$ to $3.9 \times 3.4 \times 14.6 \text{ nm}^3$ with larger x - and y -dimensions necessary for the stretched kao surfaces and larger z -dimension required for the compressed kao surfaces. Further details are provided in the [Supporting Information](#).

Each water layer placed near the kao surface consisted of 720 water molecules. The TIP4P/Ice model was used to represent water in our simulations.⁵⁰ TIP4P/Ice is shown to accurately capture the phase diagram of water and the different ice polymorphs. Kao was described by the CLAYFF force field.⁵¹ Since we are focused on elucidating the effect of lattice match and hydrogen bonding on ice nucleation, we chose to hold the positions of all the kao atoms except the hydrogen atoms of the hydroxyl groups in contact with water fixed in our simulations. The hydrogen atoms were covalently bonded to the oxygen atoms and the –OH bond length was maintained at 0.0978 nm. No constraints were imposed on the bond angles.

The initial configurations for the water molecules were taken from a simulation of bulk water at 300 K. This configuration was energy minimized, and multiple simulations were launched with velocities randomly generated from a Maxwell distribution at 300 K. The system was quenched from 300 to 230 K. This corresponds to $\sim 40 \text{ K}$ supercooling for TIP4P/Ice model. Each simulation was run for at least 1 μs in the NVT ensemble. Temperature was maintained using the V-rescale thermostat.⁵² Electrostatic interactions were calculated using the particle mesh Ewald method⁵³ as implemented in GROMACS. Bond lengths of the hydroxyl groups in kao and geometry of water molecules were constrained using the LINCS algorithm.⁵⁴ A time step of 2 fs was used, and configurations were stored every 10 ps for further analysis. All MD simulations were performed using GROMACS 4.5 and 4.6.⁵⁵

To investigate the effect of surface lattice spacing on ice nucleation, microsecond long simulations were performed on all of our modified surfaces. The surface hydroxyl groups were free to rotate around a fixed oxygen position and we refer to them as flexible. To investigate the effect of the flexibility of the surface hydroxyl groups on ice nucleation, additional simulations were performed where the –OH groups were fixed. In these simulations, the entire kao surface was frozen with the surface hydroxyl groups oriented either parallel (fixed upright) or perpendicular (fixed down) to the surface normal. We refer to these with the added subscript of up and down, respectively. A summary of the different systems simulated is provided in [Table 1](#). Collectively, a total of 60 μs of MD simulations were performed to study the effects of surface lattice, and surface hydroxyl groups on the observed ice nucleation behavior.

Table 1. Summary of the Simulations Performed and the Number of Nucleation Events Observed

surface	(x,y) nm	–OH orientation	water model	runs	nucleation events observed
kao_{-20}	(2.69,2.33)	flexible	TIP4P/Ice	17	3
kao_{-10}	(2.91,2.52)	flexible	TIP4P/Ice	6	0
kao_0	(3.23,2.80)	flexible	TIP4P/Ice	6	0
kao_{+10}	(3.56,3.08)	flexible	TIP4P/Ice	1 ^a	0
kao_{+20}	(3.88,3.36)	flexible	TIP4P/Ice	1 ^a	0
kao_{-20}	(2.69,2.33)	fixed upright	TIP4P/Ice	11	2
kao_{-20}	(2.69,2.33)	fixed down	TIP4P/Ice	6	0
kao_{-10}	(2.91,2.52)	fixed upright	TIP4P/Ice	6	0
kao_0	(3.23,2.80)	fixed upright	TIP4P/Ice	6	0

^aNo nucleation was observed at this surface, and based on the insights from nucleation at the other surfaces, we decided that this surface represented too large a lattice mismatch to observe ice nucleation. Therefore, no further simulations were performed.

3. RESULTS AND DISCUSSION

To investigate the effect of lattice spacing, we performed several microsecond long MD simulations of water on model kao surfaces at 40 K supercooling. Conventionally, surfaces with a lattice spacing close to that of ice are believed to promote ice nucleation through a templating effect. Given a structure that correlates to the hexagonal structure of the ice crystal, how close in lattice does the surface need to be to promote ice nucleation? To probe this question, we generated kao surfaces that have lattice spacings spanning from a lattice mismatch of

Table 2. Surface Specifications of the Kao Surfaces Used in This Study^a

surface	a_{surf}	r_{OO}	$\delta(\%)$	ice?
kao ₋₂₀	0.449	0.225	0.0	yes
kao ₋₁₀	0.485	0.243	8.0	no
kao ₀	0.539	0.270	20	no
kao ₊₁₀	0.593	0.297	32	no
kao ₊₂₀	0.647	0.323	44	no

^aThe lattice mismatch from I_h and I_c and the distance between the nearest oxygen atoms (r_{OO}) are shown. $r_{\text{OO,ice}} = 0.275$ nm and $a_{\text{ice}} = 0.449$ nm³⁶.

0% to 44% with the ice structure, as shown in Table 2. Lattice mismatch, δ is calculated using the relation

$$\delta(\%) = \frac{a_{\text{surf}} - a_{\text{ice}}}{a_{\text{ice}}} \times 100$$

where a_{surf} and a_{ice} are the lattice spacing of the surface and ice, respectively. The lattice spacing for the kao surfaces is equal to two times the distance between the nearest coplanar oxygen atoms. a_{ice} is equal to the distance between the nearest coplanar oxygen atoms in the basal plane of ice. These distances were selected based on the expected sites for water adsorption that were evaluated from preliminary simulations of kao₀–water systems.

3.0.1. Ice Nucleation. The density distribution of water oxygen atoms as a function of the distance from the surface was calculated to capture the changes in the water structure during the simulations. As expected, layering of water molecules is observed in all cases studied. Since all the kao surfaces are hydrophilic and have the ability to hydrogen bond with the water molecules we observe a large first peak in the density distribution. As the simulation proceeds, there is an increase in the sharpness of the layers further away from the surface for all cases. This indicates there are some local rearrangements of water molecules leading to more ordered water molecules further from the surface. Kao₋₂₀ promoted the most structuring leading to well-defined water layers further away from the surface. Double peaks separated by wide minima in the density distribution function of water molecules near kao₋₂₀ surface evolved, suggesting the development of some crystalline structure (see Figure 1a). The distance between the double peaks within a hydration layer is ~ 0.09 nm. This distance is equal to the height of the chair formation hexagons in ice. The distance between hydration layers is ~ 0.365 nm, which corresponds to the height difference of two basal layers in the ice structure. This suggests that we observe ice-like structure on kao₋₂₀ surface. No such crystalline structures were observed for the other surfaces in our 1 μ s long

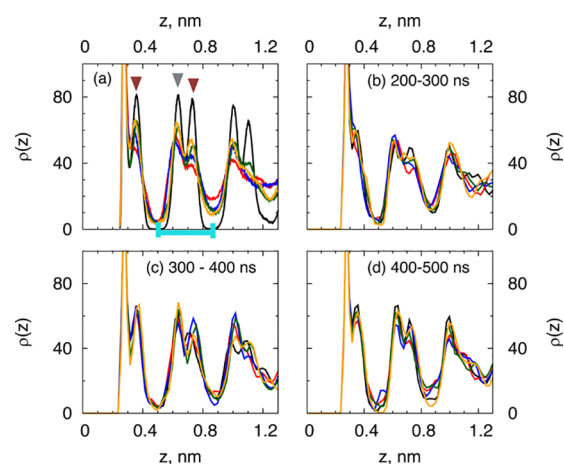


Figure 1. Representative density distribution profiles of water oxygen atoms ($\rho(z)$) as a function of distance from the kao₋₂₀ surface (z). The $z = 0$ surface is the plane of the surface hydroxyl oxygen atoms. Density profiles at different times are shown. (a) Density is averaged over 100 ns; red: 100–200 ns, blue: 200–300 ns, green: 300–400 ns, yellow: 400–500 ns, black: 500–600 ns. Cyan line indicates the second hydration layer, gray arrowhead represents the first peak of the second hydration layer, and brown arrowheads represent the second peak in the first and second hydration layers. (b–d) Each density profile corresponds to an average over 10 ns for the time range indicated. For example, in panel b, red: 200–210 ns, blue: 220–230 ns, green: 240–250 ns, orange: 260–270 ns, black: 280–290 ns.

simulations. This suggests that kao₋₂₀ is the most effective ice nucleating agent relative to the other surfaces studied here.

Using the CHILL algorithm,⁵⁷ we characterized the ice type growing on the surface. We find the growth of stacked hexagonal (I_h)–cubic (I_c) structures near the kao₋₂₀ surfaces. Previous studies have reported the formation of stacked I_h – I_c structures for homogeneous ice nucleation,^{58–62} and only I_h near kaolinite surfaces.^{22,42,43} It was argued that I_h was observed near the kaolinite surface because it supported the nucleation at the prismatic plane.^{22,42} The differences in the ice type near kaolinite and kao₋₂₀ surfaces arise from the plane of ice in contact with the surface. In contrast to kaolinite, the kao₋₂₀ surface promotes the basal plane of ice. Structurally the basal planes of I_h and I_c are the same, and there is no competition between them within this layer. Stacking disorder occurs in the direction normal to the basal plane. Thus, the growth from the basal plane can easily allow stacking disorder. On the other hand, surfaces supporting a prismatic plane could hinder stacking disorder since it would need to occur at an angle with the surface. This would, thus, result in the growth of I_h at the surface. These results highlight the potential of significant differences in ice structure arising from subtle changes in the lattice spacing and topology of the surface.

3.0.2. Mechanism of Ice Nucleation. Detailed evolution of the ice structure near the kao₋₂₀ surface as captured by the density profiles is shown in Figure 1. The structural rearrangements leading to ice nucleation and growth begin in the second hydration layer. The second hydration layer corresponds to the region between the first and second minima in the density profile, as indicated in Figure 1a. The rearrangements result in the formation of double peaks, and wide minima characteristic of ice structure. The second hydration layer develops into a bilayer, as the shoulder of the first hydration layer (gray arrowhead in Figure 1a) develops into a peak almost simultaneously. The density in the minima

decreases concurrently to the formation of the double peaks. The water molecules at the distance from the surface corresponding to the minima rearrange into the neighboring water layers as ice-like structures begin to form in the interfacial water layers. The second peaks that form are indicated by the red arrowheads in Figure 1a. The ice-like characteristics begin to appear in the third hydration layer as double peaks begin to evolve in the second hydration layer. The sequence of these changes can be observed in Figure 1, where the evolution of the double peaks in the first, second, and third hydration layers for kao₂₀ surfaces is shown for one representative nucleation trajectory. In 200–300 ns (Figure 1b), the shoulder of the first hydration layer begins to develop as a peak, while the second hydration layer also begins to develop double peaks. In 300–400 ns (Figure 1c), the double peaks continue to develop in the second hydration layer with simultaneous development of the second peak in the first hydration layer, and few signs of ice-like structure in the third hydration layer. In 400–500 ns (Figure 1d), the first and second hydration layers have developed double peaks, and the first minimum has ~ 0 density. The second minimum also displays decreased density and concurrent changes in the third hydration layer can be observed. There is a slight increase and emergence of a shoulder-like feature in the density in the third hydration layer. This leads to further restructuring of both the second and third hydration layer and to the evolution of the characteristic double peaks in both the layers. This suggests that the rearrangements leading to ice structure are initiated in the second hydration layer and evolve cooperatively between the first three hydration layers. This is also observed in the time evolution of the fraction of ice-like water molecules in the three layers (see Supporting Information Figure S3). The ice structure continues to grow from here.

We observe this mechanism in all cases where we observe ice nucleation. This suggests that ice nucleation is triggered in the layers close to the surface but not necessarily in the layer directly interacting with the surface. This is consistent with previous studies.^{22,23,44} These results indicate that the nucleating ability of a surface is related not only to the structure of water layer directly in contact with the surface but also on a few layers beyond that. The arrangement of water molecules in these layers is affected both by the surface and the surrounding water molecules. Therefore, ice nucleation at surfaces is a subtle interplay of water–surface and water–water interactions.

Further insights into the growth mechanism is obtained by studying the evolution of the water oxygen–oxygen in-plane radial distribution function. Figure 2 shows the in-plane radial distribution of water molecules within the second and third hydration layers. It is interesting to observe that the peaks corresponding to longer range arrangements (peaks at 0.68 and 0.76 nm) of the water molecules become pronounced before the shorter distance peaks (peak at 0.53 nm). This occurs because the in-plane growth progresses through the formation of chains of water molecules as shown in Figure 2c. These chains close into hexagons beginning to form the ice structure. On several occasions, we observe structures similar to Figure 2d which have incomplete hexagons. This manifests as the lack of a clear peak at 0.53 nm. The rotation or shift of just a few water molecules can complete the hexagons, as seen in Figure 2e. We also see patches of 3–4 water hexagons forming from which further growth of water chains and water hexagons ensues until a basal layer spanning the entire surface area is formed. We

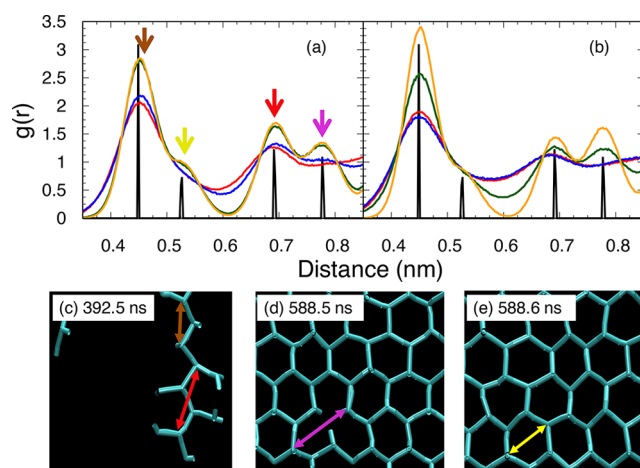


Figure 2. In-plane O–O distance within the (a) second and (b) third layers of water. The averages are taken every 100 ns; red: 300–400 ns, blue: 400–500 ns, green: 500–600 ns, orange: 900–1000 ns. Black curves indicate the in-plane $g(r)$ for perfect ice structure. Panels c–e show snapshots of structures that contribute to the different peaks highlighted in panel a.

note the complete surface coverage is perhaps due to the small surface size in our simulations. We expect that for larger surfaces the nucleus will be hemispherical. However, we surmise that within the nucleus the ice structure will evolve in a similar manner to that described here.

Observing the ice structure, as captured by the CHILL algorithm,⁵⁷ we find that the new ice layer begins to form before the previous layer is completed. Representative snapshots illustrating the growth of the first two layers of ice are shown in Figure 3. As can be seen, the ice structure in the first and second hydration layer evolves cooperatively. This suggests that the growth of ice in adjacent layers helps stabilize the in-plane chain growth to eventually form and maintain the ice structure. Chains of ice-like water molecules can also be observed (see Figure 3f–h). It is interesting to note that, while the growth of such structures was observed in homogeneous ice nucleation, they seemed to dissolve rapidly. In fact, order parameters excluding such chains captured the ice nucleation process more effectively.⁶³ By contrast, we find that these chain-like structures were precursors to the formation of larger ice patches on kao₂₀ surface. Formation of such chain-like structures occurs frequently in both bulk and interfacial water as a natural consequence of structural fluctuations in super-cooled water.⁶³ We hypothesize that the stabilization of such chains could be a mechanism through which mineral surfaces such as kao catalyze ice nucleation.

3.0.3. Orientational Analysis. Our recent findings discovered a correlation between the orientation of interfacial water molecules and the surfaces' ice nucleating ability.³⁷ Motivated by that, we studied the orientations of the water molecules near the kao surfaces. The orientations are characterized by the angle between the water dipole and surface normal. The distribution of the orientation of the water molecules in the first and second peaks of the first hydration layer and the first peak of the second hydration layer is shown in Figure 4. The first and second peaks of a given hydration layer are shown in Figure 1a. We henceforth refer to the first and second peaks of the first hydration as L1P1 and L1P2, respectively, and the first peak of the second hydration layer as L2P1.

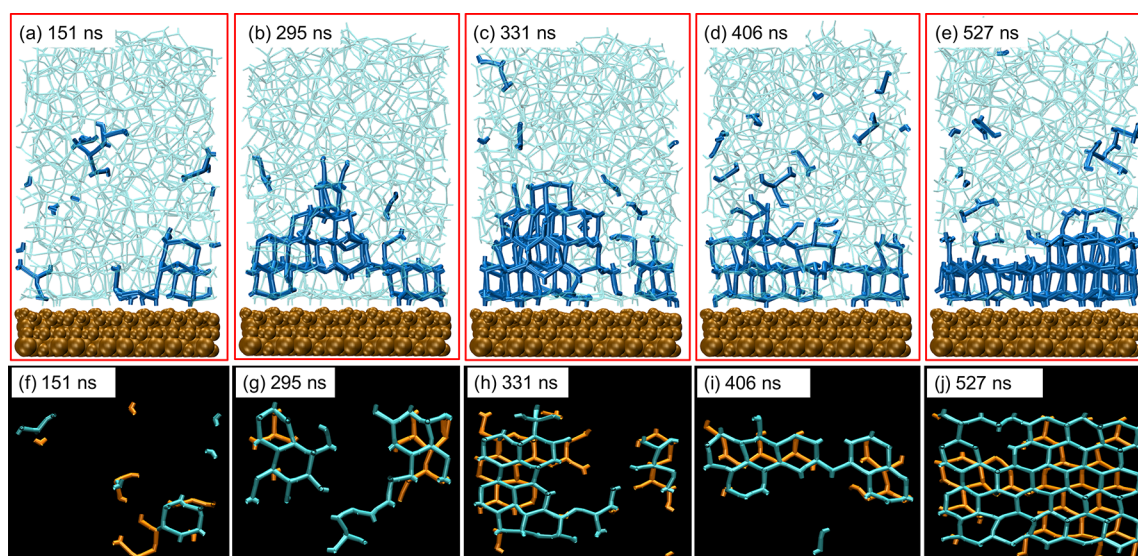


Figure 3. Time evolution of ice structure as classified by CHILL on the kao_{-20} surface. (a–e) Side view of the system. kao_{-20} surface is shown in orange and ice-like water molecules are shown in dark blue. Other water molecules are in light blue. (f–j) Top view of ice-like water molecules in the first (orange) and second (cyan) hydration layers.

Several differences in the orientations of the water molecules near kao_{-20} compared to the other kao surfaces are observed. Near the kao_{-20} surface, water molecules in L1P1 orient such that the hydrogen atoms point toward the surface. This orientation corresponds to an angle of $\sim 134^\circ$ (Figure 4a,d). The water orientations corresponding to $\sim 53\text{--}78^\circ$ are also relatively more populated near the kao_{-20} surface. On the other hand, increased sampling of orientations with angles lesser than 37° in L1P1 are observed for the other surfaces. The orientations in L1P2 are influenced by the arrangement of the water molecules in L1P1 as well as those in the second hydration layer. Near the kao_{-20} surface, peaks around $\sim 60^\circ$ and $\sim 120^\circ$ are observed. By contrast, the other surfaces promote orientations with angles $0\text{--}37^\circ$ in L1P2. Representative snapshots corresponding to these orientations are shown in Figure 4d.

These orientations in the first hydration layer influence the orientations observed in the second hydration layer. The most prominent differences in the orientations of water molecules between kao_{-20} and the other surfaces are observed in L2P1 (Figure 4c). The distribution of the orientations around angles of $\sim 134^\circ$ and $\sim 60^\circ$ is enhanced near the kao_{-20} surface. There is also a decrease in orientations corresponding to angles of $\sim 90^\circ$, $> 143^\circ$ and $< 37^\circ$. In comparison, orientations observed in L2P1 of other surfaces have higher distribution of angles of 90° , $< 37^\circ$ and $> 143^\circ$.

Promotion of ice nucleation on kao_{-20} relative to the other kao surfaces can be attributed to the differences in the orientations of interfacial water molecules. The water orientations sampled near the kao_{-20} surface, namely (i), (ii), (iii) and (iv), are also observed in the ice structure. These orientations facilitate the formation of the ice-like bilayer. In addition, they promote the hydrogen bonding between the different hydration layers promoting the growth of ice structure. This can be observed in Figure 4e, where the ice-like bilayer and hydrogen bonding between the two layers near the kao_{-20} surface can be seen. In the case of the other kao surfaces, no clear bilayer structure is observed, and the water molecules form two (single peak) hydration layers. This is the

consequence of having orientations marked as (vi) and (vii). Further, the formation of bilayer water structure is inhibited by the orientations corresponding to (v). An illustrative snapshot of water molecules near kao_0 is shown in Figure 4f.

It is interesting to note that the orientation distributions shown in Figure 4 were averaged over $0\text{--}100$ ns, and therefore correspond to the metastable liquid water structure near the surface. Ice nucleation is not observed at least until ~ 400 ns. This suggests that the structure of metastable liquid water as characterized by the orientations of the water molecules could provide a measure of the ice nucleating propensity of a surface.

3.0.4. Impact of Surface Hydroxyl Orientations. What about the kao_{-20} surface promotes the orientations favorable for an ice-like bilayer compared to the other surfaces? It could be suggested that the lattice match between kao_{-20} and ice is the primary reason for observing ice near that surface. However, previous studies have shown that lattice matching alone is insufficient for ice promotion,^{15,29,37} and that both lattice matching and hydrogen bonding contribute to kaolinite's ice nucleating abilities.^{15,29} To probe this further, we studied the orientations of the surface hydroxyl groups with respect to the surface normal (see Figure 5). The hydroxyl groups of all surfaces except kao_{-20} show peaks around 90° and 25° , which correspond to hydroxyl groups pointing into the surface and straight up, respectively. By contrast, the hydroxyl group orientation distribution shows peaks around 78° and 45° for kao_{-20} . The distribution is such that on an average two of every three hydroxyl groups orient more into the surface than toward the water layer (see Figure 5b). This arrangement supports the orientations of the water molecules observed in the first hydration layer. Interestingly, we also observe that as ice nucleation proceeds the kao_{-20} hydroxyl groups undergo some changes. Specifically, the distribution of surface hydroxyl group orientations becomes sharper (narrower) near the peaks observed at $\sim 78^\circ$ and $\sim 45^\circ$. An ability to respond to the emerging ice lattice has been suggested to enhance ice nucleation.^{11,15} This hints toward the interplay of lattice matching and surface hydroxyl group orientations in enabling ice nucleation at the kao_{-20} surface.

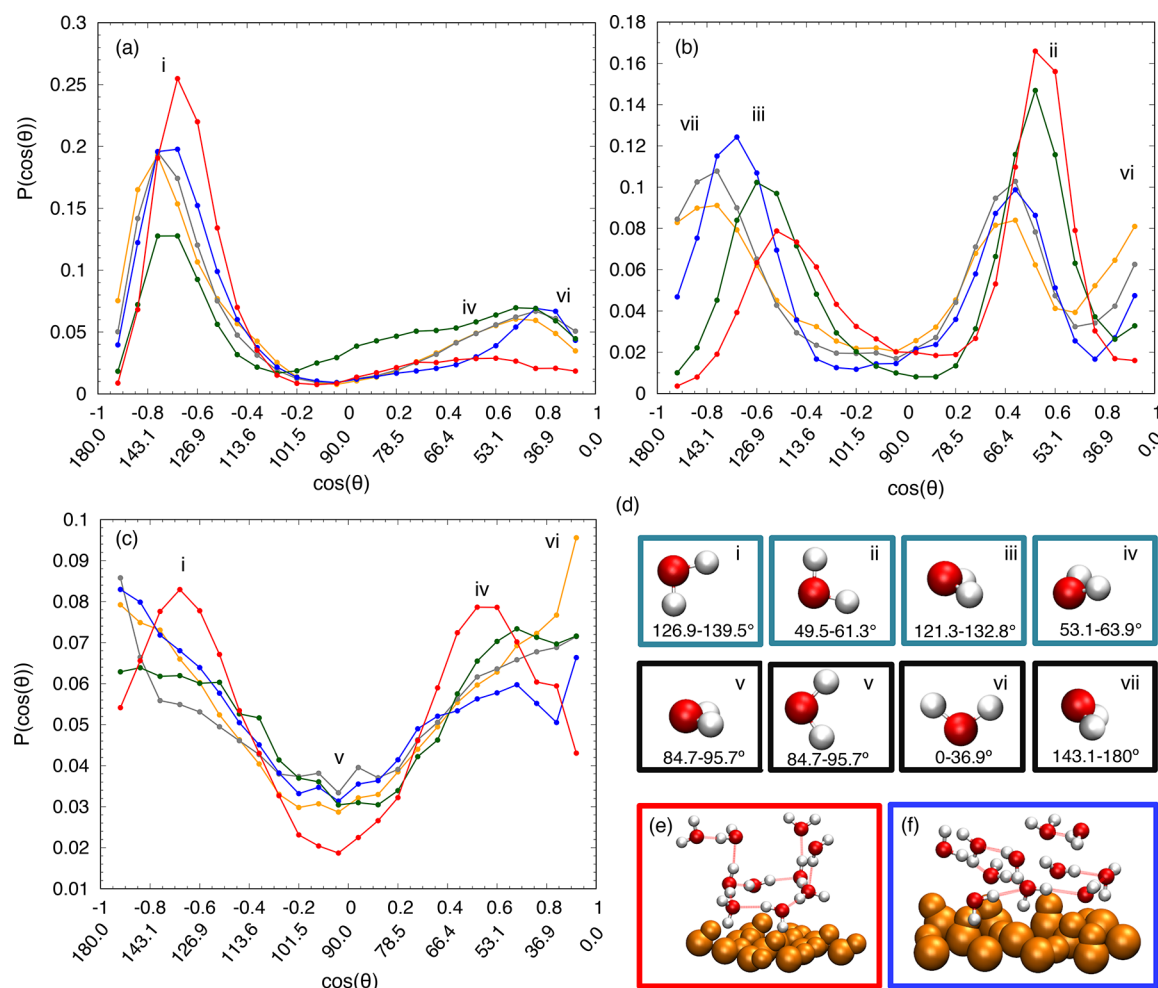


Figure 4. Dipole angle distribution with respect to the surface normal for water molecules in (a) the first peak of the first hydration layer, (b) the second peak of the first hydration layer, and (c) the first peak of the second hydration layer. The distributions are averaged over 0–100 ns. Color code: kao_{-20} – red; kao_{-10} – green; kao_0 – blue; kao_{+10} – gray; kao_{+20} – orange. (d) Representative snapshots of water molecules representing different orientations. The orientations found in ice are placed in blue boxes, and those found near the kao surfaces but not in ice are shown in black boxes. Panels e and f illustrate the structure formed by water molecules in the first two hydration layers of kao_{-20} and kao_0 surfaces, respectively. The dashed lines indicate hydrogen bonds between the water molecules.

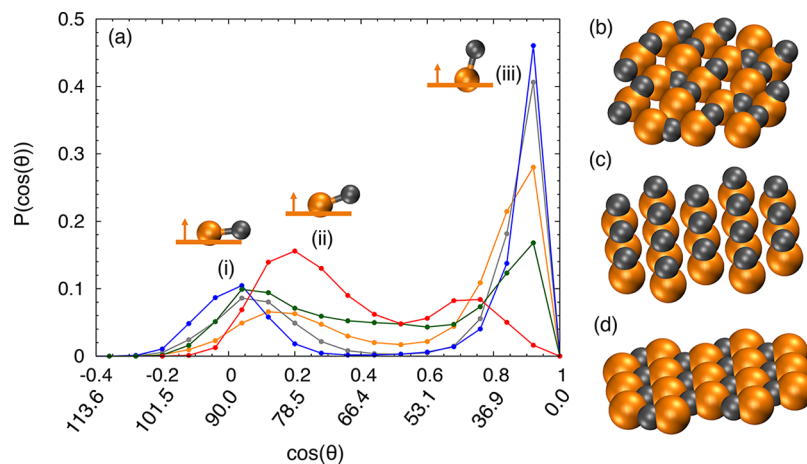


Figure 5. (a) Distribution of the angle between the surface hydroxyl groups with the surface normal. Color code: kao_{-20} – red; kao_{-10} – green; kao_0 – blue; kao_{+10} – gray; kao_{+20} – orange. Side view of the (b) kao_{-20} , (c) $kao_{-20,up}$, and (d) $kao_{-20,down}$ surfaces. Only the surface hydroxyl groups are shown where oxygen is orange and hydrogen is gray.

To further elucidate the role of the surface hydroxyl groups, we performed simulations of two kao_{-20} –water systems. In one

system, the surface hydroxyl groups were fixed in the straight up position (i.e., parallel to the surface normal), and in the

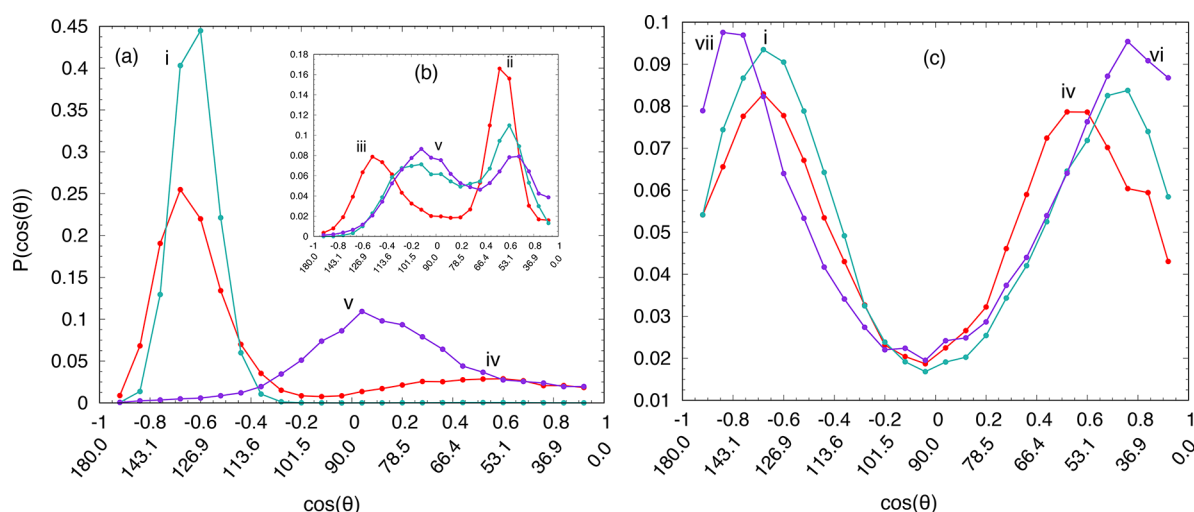


Figure 6. Distribution of angle between water dipole and surface normal for water molecules in (a) the first peak of the first hydration layer (b) second peak of the first hydration layer (c) first peak of the second hydration layer. Color code: kao_{-20} — red; $\text{kao}_{-20,\text{up}}$ — cyan; $\text{kao}_{-20,\text{down}}$ — purple.

second case the surface hydroxyl groups were fixed such that they were parallel to the surface (i.e., making 90° angle with the surface normal). We refer to these surfaces as $\text{kao}_{-20,\text{up}}$ and $\text{kao}_{-20,\text{down}}$ respectively. Snapshots of the surfaces are shown in Figure 5.

Curiously, we did not observe any ice nucleation at $\text{kao}_{-20,\text{down}}$ while ice nucleated at the $\text{kao}_{-20,\text{up}}$ surface. The mechanism of ice nucleation and growth was similar to that observed at the kao_{-20} surface. Water arrangements near the surfaces undergo changes based on the surface hydroxyl groups. Specifically, the peaks in the water density move closer to the $\text{kao}_{-20,\text{up}}$ surface relative to their location near the kao_{-20} surface, and L1P2 becomes more prominent. By contrast, the water molecules move further away from the $\text{kao}_{-20,\text{down}}$ surface and L1P2 disappears.

The distribution of the orientations of water molecules in the first and second hydration layer for the $\text{kao}_{-20,\text{up}}$ and $\text{kao}_{-20,\text{down}}$ are shown in Figure 6. In the case of $\text{kao}_{-20,\text{up}}$, the water molecules in L1P1 orient such that the hydrogen points directly toward the surface hydroxyl oxygen as indicated by the peak near orientation (i). By contrast, near $\text{kao}_{-20,\text{down}}$ the water molecules sample orientation (v), which hinders bilayer-like structure formation. Correspondingly, we do not observe any L1P2 near $\text{kao}_{-20,\text{down}}$, while there is a prominent L1P2 near $\text{kao}_{-20,\text{up}}$.

The orientations in L1P1 affect those observed in L1P2. In the case of the $\text{kao}_{-20,\text{down}}$ surface, we select the region where the second peak would be expected if there was one. Interestingly, at first glance it appears that both $\text{kao}_{-20,\text{up}}$ and $\text{kao}_{-20,\text{down}}$ surface have similar distributions. However, there are subtle differences—specifically the configurations around orientation (v) are sampled more while orientation (ii) is sampled less in $\text{kao}_{-20,\text{down}}$ relative to $\text{kao}_{-20,\text{up}}$. While orientation (v) hinders ice nucleation, orientation (ii) is favorable. In the second hydration layer (L2P1), configurations favorable for ice nucleation (orientation (i)) are observed more near the $\text{kao}_{-20,\text{up}}$ surface. It is also important to note that configurations not favorable for ice structure, orientations (vi) and (vii) are sampled lesser than in case of $\text{kao}_{-20,\text{down}}$. It is the combination of all these effects on water orientations that leads to ice nucleation at $\text{kao}_{-20,\text{up}}$ while none is observed near the $\text{kao}_{-20,\text{down}}$ surface.

To further investigate this synergistic effect of orientations on ice nucleation, we studied $\text{kao}_{-10,\text{up}}$ and $\text{kao}_{-0,\text{up}}$ surfaces (data not shown). We did not observe ice nucleation on these surfaces within one microsecond simulations. The distribution of water dipole orientation in L1P1 is similar to that seen in case of $\text{kao}_{-20,\text{up}}$ surfaces. In L1P2, orientations around (v) are sampled lesser, while sampling around orientations (ii) and (vi) is increased. In L2P1, the sampling of orientation (i) is lower, and orientations (v), (vi), and (vii) are sampled more. This emphasizes the synergy of the different orientations in indicating ice nucleating propensity. Sampling favorable orientations alone is insufficient to observe ice nucleation; it is also important that the unfavorable orientations are not sampled.

4. CONCLUSIONS

We present results elucidating the interplay of lattice matching and hydrogen bonding on the heterogeneous ice nucleation. Microsecond long molecular dynamics simulations of water in contact with model surfaces were performed. The model surfaces emulated the chemical structure of the mineral kaolinite with a layer of surface hydroxyl groups exposed to water. Ice nucleation is expected to occur at this layer. Lattice spacing and the surface hydroxyl orientation was varied. We found that ice nucleated only in cases where the lattice spacing of the model surfaces matched with that of ice. However, even with perfect lattice matching ice nucleation can be hindered by manipulating the surface hydroxyl groups. When the surface hydroxyl groups are flexible to rotate or held rigid in an “up” configuration, ice nucleation is observed. By contrast, if the surface hydroxyls are held rigid in the “down” configuration, no ice nucleation is seen. The “up” configuration has surface hydroxyls oriented parallel to the surface normal and in the “down” configuration, surface hydroxyls are perpendicular to the surface normal. This demonstrates that lattice matching and hydrogen bonding are necessary but not sufficient conditions for ice nucleation on mineral surfaces like kaolinite.

We find that ice nucleation begins in the second hydration layer. Cooperative changes in the water structure in the first and third hydration layer occur simultaneously during the nucleation process. This structure in these layers are affected by water–surface and water–water interactions. We capture this

interplay by characterizing the orientations of the metastable liquid water in the vicinity of the surfaces. We find that sampling orientations favorable for bilayer formation alone does not result in ice nucleation. It is a synergistic effect of orientations—sampling favorable and not sampling unfavorable configurations—that leads to ice nucleation. Such a balance of orientations can be easily perturbed by subtle changes to the surface properties. The complex relationship between surface properties and interfacial water structure results in the complexity of heterogeneous ice nucleation reported. These results in combination with our previous results on AgI surface³⁷ suggest that water orientation of metastable liquid in contact with a surface can provide a measure to ascertain whether the surface is a good or bad ice nucleating agent. Further studies to investigate this correlation over a broader range of surfaces is currently underway in our group. Additionally, the necessity of running long microsecond long MD simulations to observe ice nucleation limits the number of nucleation events we can sample. To address this, various advanced sampling techniques such as transition path sampling,⁶⁴ transition interface sampling,⁶⁵ and forward flux sampling⁶⁶ can be used. This will enable sampling of statistically relevant number of nucleation events thereby, providing data for further developing correlations between ice nucleation and water structure. Such efforts, specifically using forward flux sampling to study ice nucleation, are currently being pursued in our research group.

■ ASSOCIATED CONTENT

Supporting Information

The Supporting Information is available free of charge on the ACS Publications website at DOI: [10.1021/acs.langmuir.7b02859](https://doi.org/10.1021/acs.langmuir.7b02859).

Details of the kao surfaces and the MD simulations, and evolution of ice-like water molecules in the water layers (PDF)

■ AUTHOR INFORMATION

Corresponding Author

*E-mail: ssarupr@clemson.edu.

ORCID

Sapna Sarupria: 0000-0001-7692-8313

Notes

The authors declare no competing financial interest.

■ ACKNOWLEDGMENTS

S.S. gratefully acknowledges financial support from Clemson University start-up funds and NSF grant #1541944. We thank the Clemson Cyberinfrastructure Technology Integration group for allocation of computing time on the Palmetto Cluster. We also thank Dr. Gren Patey (The University of British Columbia) for sharing his files on kaolinite with us and for insightful discussions.

■ REFERENCES

- (1) Sharp, K. A peek at ice binding by antifreeze proteins. *Proc. Natl. Acad. Sci. U. S. A.* **2011**, *108*, 7281–7282.
- (2) Liou, Y.; Tocilj, A.; Davies, P.; Jia, Z. Mimicry of ice structure by surface hydroxyls and water of a bold beta-helix antifreeze protein. *Nature* **2000**, *406*, 322–324.

- (3) Christner, B.; Morris, C.; Foreman, C.; Cai, R.; Sands, D. Ubiquity of Biological Ice Nucleators in Snowfall. *Science* **2008**, *319*, 1214.
- (4) Kawahara, H. The structures and functions of ice crystal-controlling proteins from bacteria. *J. Biosci. Bioeng.* **2002**, *94*, 492–496.
- (5) Lintunen, A.; Hölttä, T.; Kulmala, M. Anatomical regulation of ice nucleation and cavitation helps trees to survive freezing and drought stress. *Sci. Rep.* **2013**, *3*, 2031.
- (6) Li, B.; Sun, D. Novel methods for rapid freezing and thawing of foods—a review. *J. Food Eng.* **2002**, *54*, 175–182.
- (7) Murray, B. J.; O'Sullivan, D.; Atkinson, J. D.; Webb, M. E. Ice nucleation by particles immersed in supercooled cloud droplets. *Chem. Soc. Rev.* **2012**, *41*, 6519–6554.
- (8) Atkinson, J.; Murray, B.; Woodhouse, M.; Whale, T.; Baustian, K.; Carslaw, K.; Dobbie, S.; O'Sullivan, D.; Malkin, T. The importance of feldspar for ice nucleation by mineral dust in mixed-phase clouds. *Nature* **2013**, *498*, 355–358.
- (9) Pruppacher, H. R.; Klett, J. D. *Microphysics of Clouds and Precipitation*, 2nd ed.; Kluwer Academic Publishers: Dordrecht, The Netherlands, 1997.
- (10) Hegg, D. A.; Baker, M. B. Nucleation in the atmosphere. *Rep. Prog. Phys.* **2009**, *72*, 056801.
- (11) Cantrell, W.; Robinson, C. Heterogeneous freezing of ammonium sulfate and sodium chloride solutions by long chain alcohols. *Geophys. Res. Lett.* **2006**, *33*, L07802.
- (12) Ochshorn, E.; Cantrell, W. Ice nucleation on hydrophilic silicon. *J. Chem. Phys.* **2008**, *128*, 134701.
- (13) Ochshorn, E.; Cantrell, W. Towards understanding ice nucleation by long chain alcohols. *J. Chem. Phys.* **2006**, *124*, 054714.
- (14) Zimmermann, F.; Ebert, M.; Worringer, A.; Schütz, L.; Weinbruch, S. Environmental scanning electron microscopy (ESEM) as a new technique to determine the ice nucleation capability of individual atmospheric aerosol particles. *Atmos. Environ.* **2007**, *41*, 8219–8227.
- (15) Zielke, S. A.; Bertram, A. K.; Patey, G. N. Simulations of Ice Nucleation by Model AgI Disks and Plates. *J. Phys. Chem. B* **2016**, *120*, 2291–2299.
- (16) Zielke, S. A.; Bertram, A. K.; Patey, G. N. A molecular mechanism of ice nucleation on model AgI surfaces. *J. Phys. Chem. B* **2015**, *119*, 9049–9055.
- (17) Fraux, G.; Doye, P. Note: Heterogeneous ice nucleation on silver-iodide-like surfaces. *J. Chem. Phys.* **2014**, *141*, 216101.
- (18) Connolly, P.; Möhler, O.; Field, P.; Saathoff, H.; Burgess, R.; Choularton, T.; Gallagher, M. Studies of heterogeneous freezing by three different desert dust samples. *Atmos. Chem. Phys.* **2009**, *9*, 2805–2824.
- (19) Salam, A.; Lohmann, U.; Crenna, B.; Lesins, G.; Klages, P.; Rogers, D.; Irani, R.; MacGillivray, A.; Coffin, M. Ice Nucleation Studies of Mineral Dust Particles with a New Continuous Flow Diffusion Chamber. *Aerosol Sci. Technol.* **2006**, *40*, 134–143.
- (20) Hoose, C.; Möhler, O. Heterogeneous ice nucleation on atmospheric aerosols: a review of results from laboratory experiments. *Atmos. Chem. Phys.* **2012**, *12*, 9817–9854.
- (21) Cox, S. J.; Kathmann, S. M.; Purton, J. A.; Gillan, M. J.; Michaelides, A. Non-hexagonal ice at hexagonal surfaces: the role of lattice mismatch. *Phys. Chem. Chem. Phys.* **2012**, *14*, 7944–7949.
- (22) Cox, S.; Raza, Z.; Kathmann, S.; Slater, B.; Michaelides, A. The microscopic features of heterogeneous ice nucleation may affect the macroscopic morphology of atmospheric ice crystals. *Faraday Discuss.* **2014**, *167*, 389–403.
- (23) Lupi, L.; Molinero, V. Does Hydrophilicity of Carbon Particles Improve Their Ice Nucleation Ability? *J. Phys. Chem. A* **2014**, *118*, 7330–7337.
- (24) Croteau, T.; Bertram, A. K.; Patey, G. N. Adsorption and Structure of Water on Kaolinite Surfaces: Possible Insight into Ice Nucleation from Grand Canonical Monte Carlo Calculations. *J. Phys. Chem. A* **2008**, *112*, 10708–10712.

- (25) Croteau, T.; Bertram, A. K.; Patey, G. N. Simulation of Water Adsorption on Kaolinite under Atmospheric Conditions. *J. Phys. Chem. A* **2009**, *113*, 7826–7833.
- (26) Croteau, T.; Bertram, A. K.; Patey, G. N. Observations of High-Density Ferroelectric Ordered Water in Kaolinite Trenches using Monte Carlo Simulations. *J. Phys. Chem. A* **2010**, *114*, 8396–8405.
- (27) Carrasco, J.; Hodgson, A.; Michaelides, A. A molecular perspective of water at metal interfaces. *Nat. Mater.* **2012**, *11*, 667–674.
- (28) Feibelman, P. J. The first wetting layer on a solid. *Phys. Today* **2010**, *63*, 34–39.
- (29) Hu, X. L.; Michaelides, A. Ice formation on kaolinite: Lattice match or amphoterism? *Surf. Sci.* **2007**, *601*, 5378–5381.
- (30) Cox, S. J.; Kathmann, S. M.; Slater, B.; Michaelides, A. Molecular simulations of heterogeneous ice nucleation. I. Controlling ice nucleation through surface hydrophilicity. *J. Chem. Phys.* **2015**, *142*, 184704.
- (31) Cox, S. J.; Kathmann, S. M.; Slater, B.; Michaelides, A. Molecular simulations of heterogeneous ice nucleation. II. Peeling back the layers. *J. Chem. Phys.* **2015**, *142*, 184705.
- (32) Reinhardt, A.; Doye, J. P. Effects of surface interactions on heterogeneous ice nucleation for a monatomic water model. *J. Chem. Phys.* **2014**, *141*, 084501.
- (33) Fitzner, M.; Sossio, G. C.; Cox, S. J.; Michaelides, A. The Many Faces of Heterogeneous Ice Nucleation: Interplay Between Surface Morphology and Hydrophobicity. *J. Am. Chem. Soc.* **2015**, *137*, 13658–13669.
- (34) Pedevilla, P.; Cox, S. J.; Slater, B.; Michaelides, A. Can Ice-Like Structures Form on Non-Ice-Like Substrates? The Example of the K-feldspar Microcline. *J. Phys. Chem. C* **2016**, *120*, 6704–6713.
- (35) Bi, Y.; Cabriolu, R.; Li, T. Heterogeneous ice nucleation controlled by the coupling of surface crystallinity and surface hydrophilicity. *J. Phys. Chem. C* **2016**, *120*, 1507–1514.
- (36) Moore, E. B.; de la Llave, E.; Welke, K.; Scherlis, D. A.; Molinero, V. Freezing, melting and structure of ice in a hydrophilic nanopore. *Phys. Chem. Chem. Phys.* **2010**, *12*, 4124–4134.
- (37) Glatz, B.; Sarupria, S. The surface charge distribution affects the ice nucleating efficiency of silver iodide. *J. Chem. Phys.* **2016**, *145*, 211924.
- (38) Singh, J.; Müller-Plathe, F. On the characterization of crystallization and ice adhesion on smooth and rough surfaces using molecular dynamics. *Appl. Phys. Lett.* **2014**, *104*, 021603.
- (39) Bi, Y.; Cao, B.; Li, T. Enhanced heterogeneous ice nucleation by special surface geometry. *Nat. Commun.* **2017**, *8*, 15372.
- (40) Cabriolu, R.; Li, T. Ice nucleation on carbon surface supports the classical theory for heterogeneous nucleation. *Phys. Rev. E* **2015**, *91*, 052402.
- (41) Qiu, Y.; Odendahl, N.; Hudait, A.; Mason, R.; Bertram, A. K.; Paesani, F.; DeMott, P. J.; Molinero, V. Ice nucleation efficiency of hydroxylated organic surfaces is controlled by their structural fluctuations and mismatch to ice. *J. Am. Chem. Soc.* **2017**, *139*, 3052–3064.
- (42) Zielke, S. A.; Bertram, A. K.; Patey, G. N. Simulations of ice nucleation by kaolinite (001) with rigid and flexible surfaces. *J. Phys. Chem. B* **2016**, *120*, 1726–1734.
- (43) Sossio, G. C.; Li, T.; Donadio, D.; Tribello, G. A.; Michaelides, A. Microscopic Mechanism and Kinetics of Ice Formation at Complex Interfaces: Zooming in on Kaolinite. *J. Phys. Chem. Lett.* **2016**, *7*, 2350–2355.
- (44) Lupi, L.; Hudait, A.; Molinero, V. Heterogeneous nucleation of ice on carbon surfaces. *J. Am. Chem. Soc.* **2014**, *136*, 3156–3164.
- (45) Sossio, G. C.; Tribello, G. A.; Zen, A.; Pedevilla, P.; Michaelides, A. Ice formation on kaolinite: Insights from molecular dynamics simulations. *J. Chem. Phys.* **2016**, *145*, 211927.
- (46) Caquineau, S.; Gaudichet, A.; Gomes, L.; Magonthier, M.-C.; Chatenet, B. Saharan dust: Clay ratio as a relevant tracer to assess the origin of soil-derived aerosols. *Geophys. Res. Lett.* **1998**, *25*, 983–986.
- (47) Bish, D. L. Rietveld refinement of the kaolinite structure at 1.5 K. *Clays Clay Miner.* **1993**, *41*, 738–744.
- (48) Teppen, B. J.; Rasmussen, K.; Bertsch, P. M.; Miller, D. M.; Schäfer, L. Molecular dynamics modeling of clay minerals. 1. Gibbsite, kaolinite, pyrophyllite, and beidellite. *J. Phys. Chem. B* **1997**, *101*, 1579–1587.
- (49) Delville, A. Monte Carlo Simulations of Surface Hydration: An Application to Clay Wetting. *J. Phys. Chem.* **1995**, *99*, 2033–2037.
- (50) Abascal, J. L. F.; Sanz, E.; García Fernández, R.; Vega, C. A potential model for the study of ice and amorphous water: TIP4P/Ice. *J. Chem. Phys.* **2005**, *122*, 234511.
- (51) Cygan, R. T.; Liang, J.; Kalinichev, A. G. Molecular Models of Hydroxide, Oxyhydroxide, and Clay Phases and the Development of a General Force Field. *J. Phys. Chem. B* **2004**, *108*, 1255–1266.
- (52) Bussi, G.; Donadio, D.; Parrinello, M. Canonical sampling through velocity rescaling. *J. Chem. Phys.* **2007**, *126*, 014101.
- (53) Darden, T.; York, D.; Pedersen, L. Particle mesh Ewald: An Nlog(N) method for Ewald sums in large systems. *J. Chem. Phys.* **1993**, *98*, 10089–10092.
- (54) Hess, B.; Bekker, H.; Berendsen, H. J. C.; Fraaije, J. G. E. M. LINCS: a linear constraint solver for molecular simulations. *J. Comput. Chem.* **1997**, *18*, 1463–1472.
- (55) Pronk, S.; Pall, S.; Schulz, R.; Larsson, P.; Bjelkmar, P.; Apostolov, R.; Shirts, M. R.; Smith, J. C.; Kasson, P. M.; van der Spoel, D. e.; et al. GROMACS 4.5: a high-throughput and highly parallel open source molecular simulation toolkit. *Bioinformatics* **2013**, *29*, 845–854.
- (56) Hobbs, P. V. *Ice Physics*; Oxford University Press: Oxford, 2010.
- (57) Moore, E. B.; de la Llave, E.; Welke, K.; Scherlis, D.; Molinero, V. Freezing, melting and structure of ice in a hydrophilic nanopore. *Phys. Chem. Chem. Phys.* **2010**, *12*, 4124–4134.
- (58) Malkin, T. L.; Murray, B. J.; Salzmänn, C. G.; Molinero, V.; Pickering, S. J.; Whale, T. F. Stacking disorder in ice I. *Phys. Chem. Chem. Phys.* **2015**, *17*, 60–76.
- (59) Murray, B. J.; Malkin, T. L.; Salzmänn, C. G. The crystal structure of ice under mesospheric conditions. *J. Atmos. Sol.-Terr. Phys.* **2015**, *127*, 78–82.
- (60) Johnston, J. C.; Molinero, V. Crystallization, melting, and structure of water nanoparticles at atmospherically relevant temperatures. *J. Am. Chem. Soc.* **2012**, *134*, 6650–6659.
- (61) Kuhs, W. F.; Sippel, C.; Falenty, A.; Hansen, T. C. Extent and relevance of stacking disorder in ice Ic. *Proc. Natl. Acad. Sci. U. S. A.* **2012**, *109*, 21259–21264.
- (62) Haji-Akbari, A.; DeBenedetti, P. G. Direct calculation of ice homogeneous nucleation rate for a molecular model of water. *Proc. Natl. Acad. Sci. U. S. A.* **2015**, *112*, 10582–10588.
- (63) Reinhardt, A.; Doye, P. K. J.; Noya, E. G.; Vega, C. Local order parameters for use in driving homogeneous ice nucleation with all-atom models of water. *J. Chem. Phys.* **2012**, *137*, 194504.
- (64) Bolhuis, P. G.; Chandler, D.; Dellago, C.; Geissler, P. L. Transition path sampling: Throwing ropes over rough mountain passes, in the dark. *Annu. Rev. Phys. Chem.* **2002**, *53*, 291–318.
- (65) van Erp, T. S.; Bolhuis, P. G. Elaborating transition interface sampling methods. *J. Comput. Phys.* **2005**, *205*, 157–181.
- (66) Allen, R. J.; Valeriani, C.; Rein ten Wolde, P. Forward flux sampling for rare event simulations. *J. Phys.: Condens. Matter* **2009**, *21*, 463102.